ISSN 0020-1685, Inorganic Materials, 2018, Vol. 54, No. 2, pp. 208–219. © Pleiades Publishing, Ltd., 2018.
Original Russian Text © A.V. Stepanov, A.A. Bush, K.E. Kamentsev, 2018, published in Neorganicheskie Materialy, 2018, Vol. 54, No. 2, pp. 221–238.

Phase Diagram and Dielectric Properties of $(1-x)Ba(Ti_{1-y}Zr_y)O_3 \cdot xPbTiO_3$ Ceramics

A. V. Stepanov, A. A. Bush*, and K. E. Kamentsev

Moscow Technological University (Moscow Institute of Radio Engineering, Electronics, and Automation), pr. Vernadskogo 78, Moscow, 119454 Russia

**e-mail: aabush@yandex.ru*

Received May 3, 2017; in final form, September 5, 2017

Abstract—Ceramic $(1-x)Ba(Ti_{1-y}Zr_y)O_3 \cdot xPbTiO_3$ ($0 \le x, y \le 1$) samples have been characterized by X-ray diffraction and dielectric measurements. The results have been used to map out the phase diagram of the system, which demonstrates the variation in the phase composition of the samples. It has been shown that, in the composition regions adjacent to the $BaTiO_3$–$PbTiO_3$ side and $BaZrO_3$ corner of the composition triangle, the samples consist of perovskite solid solutions that have tetragonal and cubic structures, respectively, at room temperature. In the intermediate composition region, the samples consist of different perovskite solid solutions similar in composition and structure. We have obtained composition dependences of the unit-cell symmetry and parameters for the solid solutions, their ferroelectric Curie temperature T_C, characteristic dielectric relaxation temperatures, dielectric permittivity ε, and dielectric loss tangent $\tan\delta$ (at temperatures from 100 to 800 K and frequencies from 25 to 10^6 Hz) and analyzed the evolution of their dielectric properties with increasing $BaZrO_3$ content: from ferroelectric to properties of ferroelectric relaxors, reentrant relaxors, and dielectric relaxors of the dipole glass type.

Keywords: ferroelectric ceramics, solid solutions, perovskite structure, phase diagram, dielectric properties, dielectric relaxation

DOI: 10.1134/S0020168518020140

INTRODUCTION

The physical properties of $Ba(Ti_{1-y}Zr_y)O_3$ (BTZ) solid solutions ($0 \le y \le 1$) with the perovskite structure are of both scientific and practical interest, so these materials have been the subject of intense research in the past few decades [1–10]. As the Zr content of these solid solutions increases, their properties sequentially change from ferroelectric, similar to those of $BaTiO_3$ (BT), in the range $0 \le y < 0.15$ to properties of ferroelectrics with a diffuse phase transition in the range $y \approx 0.15$–0.25, ferroelectric relaxors in the range $y \approx 0.25$–0.75, and dipole glass in the range $y \approx 0.75$–0.95, and properties similar to those of $BaZrO_3$ (BZ) in the range $\approx 0.95 < y \le 1$. Dielectric BZ has a relatively low dielectric permittivity ($\varepsilon \approx 30$) and behaves as an incipient ferroelectric with a monotonic increase in ε, whose cubic symmetry persists as the temperature is lowered to absolute zero [4, 5]. The BTZ solid solutions have high dielectric permittivity ε, low dielectric losses $\tan\delta$, high dielectric nonlinearity, and a good resistance to high electrical voltages [1–6]. Owing to this, they find application in the fabrication of capacitors and varicaps [3], dynamic random access memory (DRAM) devices [2], and electric-field-controlled microwave devices (phase shifters, filters, antennas, and others [3, 6]). Varying the composition of BTZ allows one to tune the electrical characteristics of the solid solutions over a wide range, which offers the possibility of optimizing their performance for a variety of applications.

Because of the proximity of the Curie point T_C of the BTZ materials to room temperature, they have a relatively large temperature coefficient of their dielectric permittivity and low spontaneous polarization P_s, which is a serious drawback in a number of applications. Since the $PbTiO_3$ (PT) phase, isostructural with barium titanate, exhibits pronounced ferroelectric properties and has high T_C (490°C) [1, 3], it is reasonable to expect that increasing the percentage of PT in $(1-x)BTZ \cdot xPT$ solid solutions will raise their T_C and P_s, without significant changes in their dielectric properties. There is little data on the properties of the $(1-x)BTZ \cdot xPT$ materials, limited to results for the constituent binaries BTZ [1–10], $(Ba_{1-u}Pb_u)TiO_3$ [1], and $(1-x)BZ \cdot xPT$ [11] and for a number of compositions in the $(1-x)BTZ \cdot xPT$ ternary system [12, 13]. Neither the phase diagram nor materials of this system have been systematically studied.

In this paper, we report the preparation of $(1 - x)$-$Ba(Ti_{1-y}Zr_y)O_3 \cdot xPbTiO_3$ materials over the entire composition region $0 \le x, y \le 1$, their structural and dielectric properties, and phase relations in this system.

EXPERIMENTAL PROCEDURE AND RESULTS

Preparation of ceramics. $(1 - x)Ba(Ti_{1-y}Zr_y)O_3 \cdot xPbTiO_3$ samples with $0 \le x, y \le 1$ were prepared in air by a standard ceramic processing route using the following starting chemicals: TiO_2 (extrapure grade), ZrO_2 (extrapure grade), PbO (analytical grade), and $BaCO_3$ (analytical grade). The compositions of the samples synthesized and characterized in this study are represented by circles in the composition triangle of the BT–BZ–PT system in Fig. 1.

Appropriate mixtures of these chemicals were homogenized by grinding with ethanol in an agate mortar. The homogenized mixtures were fired at temperatures from 1200 to 1500°C for 8 h in an SNOL 12/16 electric compartment furnace with several intermediate coolings and grindings of the firing products. The firing temperature of the $x = 1$ mixture was 1200°C. With increasing BT and BZ concentrations in the samples, the firing temperature was raised to 1350 and 1500°C, respectively.

X-ray diffraction characterization showed that the BZ-rich samples synthesized below 1400°C consisted of a mixture of the BT and BZ phases. Phase-pure $(1 - x)BTZ \cdot xPT$ solid solutions were obtained at $t \ge$ 1500°C because of the higher activation energy for the formation of BTZ in comparison with BT and BZ [14].

The synthesis products were ground and pressed at ≈15 MPa into cylindrical green compacts ≈10 mm in diameter and 1–3 mm in thickness, which were then sintered between 1250 and 1500°C for 2–4 h. As a result, we obtained ceramic samples ranging in density from 80 to 95% of theoretical density. Electrical contacts for dielectric measurements were made on the faces of the ceramic disks by firing Ag-containing paste.

X-ray diffraction characterization. The phase composition of the samples was determined by X-ray diffraction on a DRON-3 automated diffractometer (filtered copper or cobalt radiation), using powdered Ge crystals as an internal standard. The position and intensities of reflections in the X-ray diffraction patterns of the ceramic samples were consistent with those expected for $BaTiO_3$-, $BaZrO_3$-, and $PbTiO_3$-based solid solutions with the perovskite structure [15].

According to the X-ray diffraction results, the composition triangle of the BT–BZ–PT system can be divided into three regions (Fig. 1). In two regions, adjacent to the BT–PT side and BZ corner, at 296 K

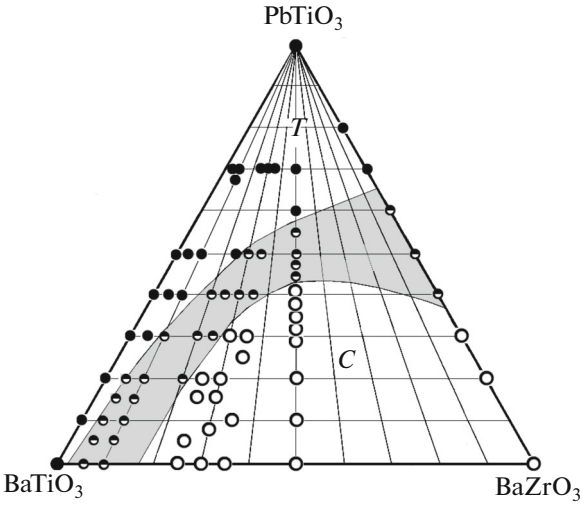

Fig. 1. Schematic of room-temperature phase relations in the $BaTiO_3$–$BaZrO_3$–$PbTiO_3$ system. The filled, open, and half-filled data points represent the compositions of the samples consisting of tetragonal (T) solid solutions, cubic (C) solid solutions, and a mixture of different solid solutions. The shaded composition region corresponds to mixtures of different solid solutions similar in composition and structure.

the samples were single-phase and consisted of perovskite solid solutions with a tetragonal (T) and a cubic (C) structure, respectively. Raising the PT content of the samples in these regions leads to a nearly linear decrease in the unit-cell parameters of the solid solutions (Figs. 2a–5a), which is obviously caused by the substitution of Pb^{2+}, a smaller sized cation (1.19 Å), for Ba^{2+} (1.35 Å) [16] in the perovskite structure of the solid solutions.

In the third, intermediate composition region, located between the first two regions, the samples consist of a mixture of different perovskite solid solutions similar in composition and structure. Since the solid solutions coexisting in the intermediate composition region differ little in unit-cell parameters, the reflections in their X-ray diffraction patterns overlap with each other, making it difficult to accurately determine their unit-cell symmetry and parameters.

To locate the phase boundaries of the tetragonal and cubic solid solutions, we used not only the X-ray diffraction data for our samples but also dielectric measurements. We took into account that the samples containing tetragonal solid solutions had a maximum in the temperature dependence of their dielectric permittivity, $\varepsilon(T)$, above 300 K, which corresponded to a ferroelectric phase transition. The $\varepsilon(T)$ curves of the cubic solid solutions had no such maxima.

Dielectric measurements were performed at temperatures from 100 to 750 K and frequencies from

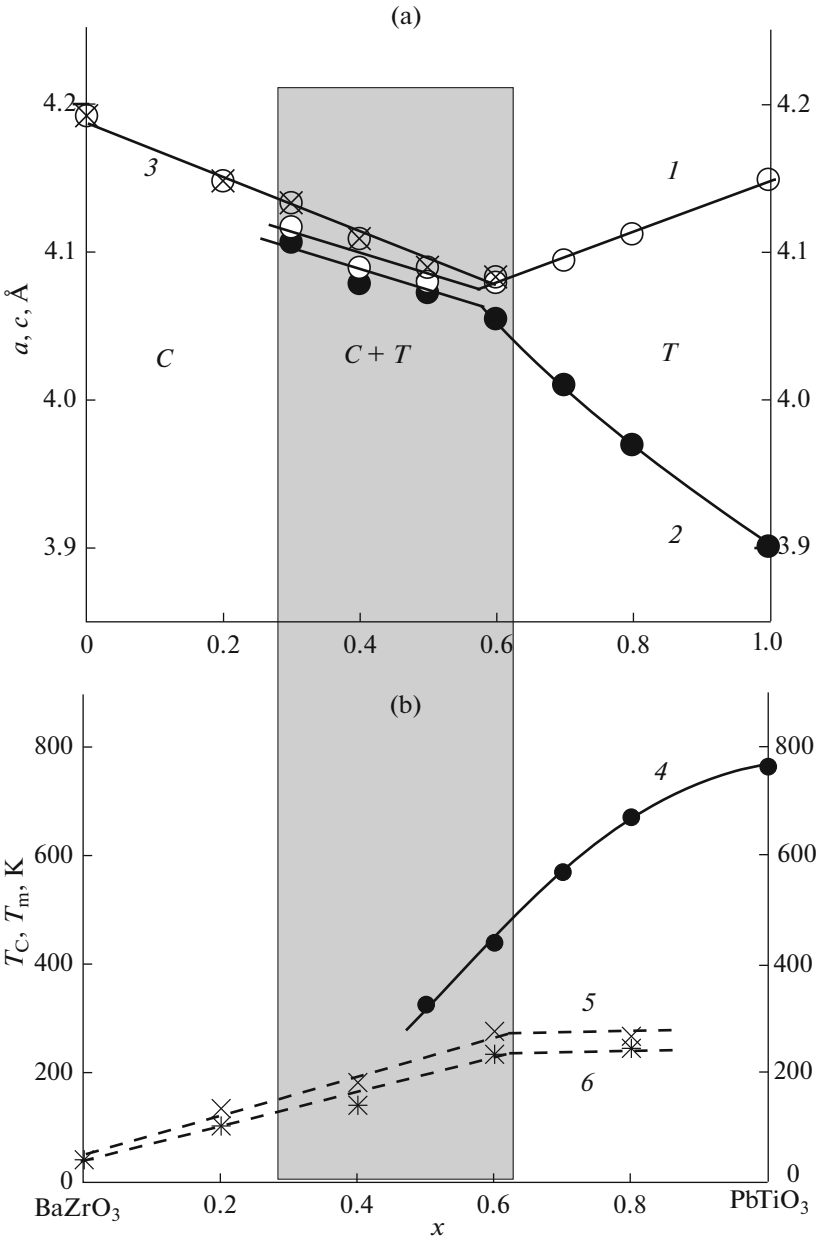

Fig. 2. Composition dependences of (a) the tetragonal (T) and cubic (C) unit-cell parameters [(*1*) a_T, (*2*) c_T, and (*3*) a_C], (b) (*4*) the Curie temperature T_C, and (*5*, *6*) the temperatures of the relaxation peaks, T_m, in the $\varepsilon(T)$ curves obtained at frequencies of 25 Hz and 1 MHz, respectively, for the $(1-x)BaZrO_3 \cdot xPbTiO_3$ solid solutions with the perovskite structure. The shaded area corresponds to the coexistence of different solid solutions.

25 Hz to 1 MHz using an E7-20 LCR meter. The results are presented in Figs. 2b–5b and 6–10.

The temperature dependences of the dielectric permittivity $\varepsilon(T)$ and dielectric loss tangent $\tan\delta(T)$ for all of the samples studied here have anomalies in the form of maxima. The curves have one, two, or three maxima, depending on the sample composition, which are reproducible in repeated measurements (Figs. 6–10). The maxima observed between 300 and 373 K in the $\varepsilon(T)$ and $\tan\delta(T)$ curves obtained during the first heating (Figs. 6, 7, 9a, 9b, 9e, 9f, 10c–10f) were not reproduced during cooling. They were most likely due to the vaporization of hygroscopic moisture, as suggested by thermogravimetric analysis data obtained using an MOM Paulik–Paulik–Erdey Q-1500 thermoanalytical system (Fig. 11). For this reason, some of the curves in Figs. 9 and 10 have discontinuities, due to the fact that these curves consist of two portions

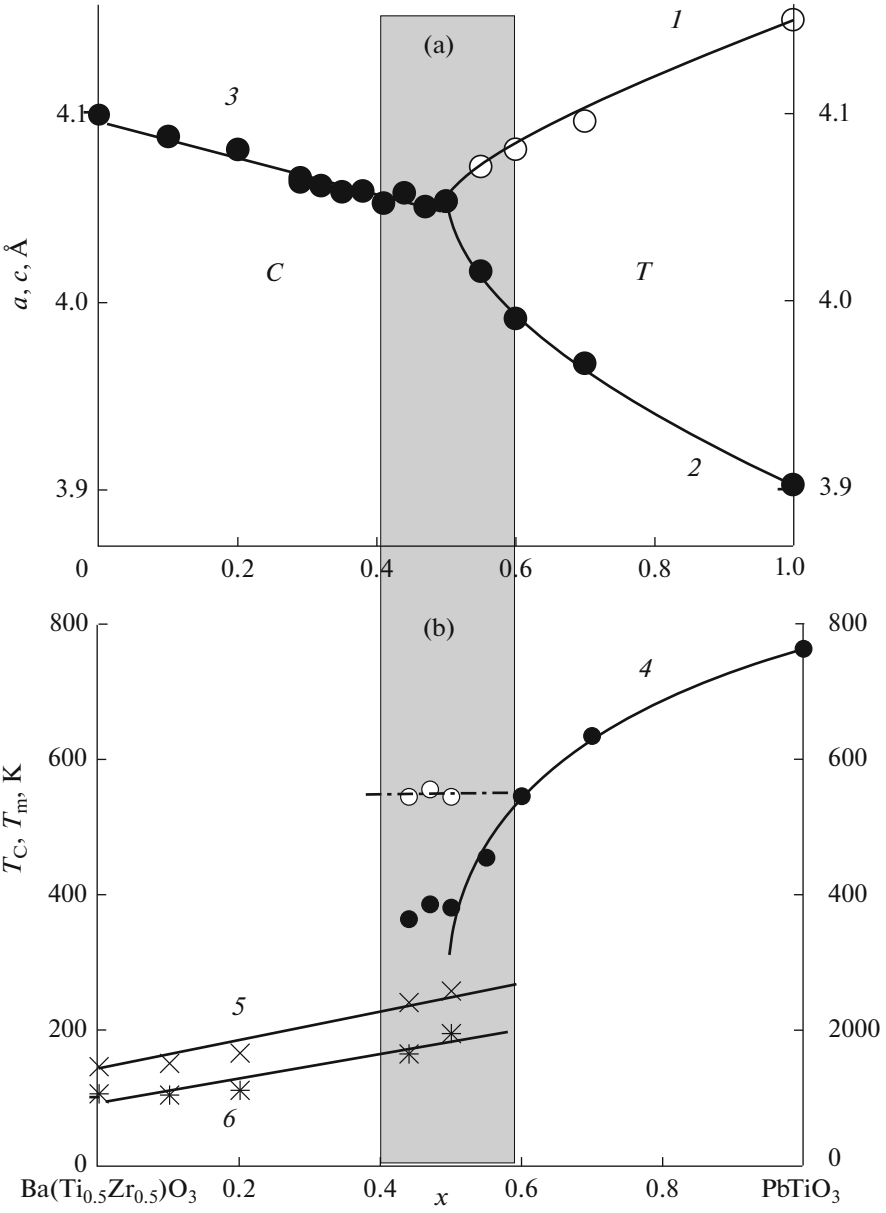

Fig. 3. Composition dependences of (a) the tetragonal (T) and cubic (C) unit-cell parameters [(*1*) a_T, (*2*) c_T, and (*3*) a_C], (b) (*4*) the Curie temperature T_C, and (*5*, *6*) the temperatures of the relaxation peaks, T_m, in the $\varepsilon(T)$ curves obtained at frequencies of 25 Hz and 1 MHz, respectively, for the $(1-x)BaTi_{0.5}Zr_{0.5}O_3 \cdot xPbTiO_3$ solid solutions with the perovskite structure. The shaded area corresponds to the coexistence of different solid solutions.

obtained using results of two distinct measurements: at high temperatures, in the range 290–750 K, and at low temperatures, in the range from 100 to ~400 K. The low-temperature measurements were performed after the high-temperature ones, so the corresponding curves did not have any maxima in $\varepsilon(T)$ or tan $\delta(T)$ near 100°C attributable to hygroscopic moisture vaporization.

The position of the high-temperature peak in the $\varepsilon(T)$ curve (and in the $\tan\delta(T)$ curve) of our samples is independent of the measuring field frequency (Figs. 9, 10). The peak is due to the ferroelectric phase transition of the solid solutions, as supported by quasi-static pyroelectric measurements made as described previously [13]. Clearly, the temperature of the peak in the $\varepsilon(T)$ curve corresponds to the Curie temperature T_C of ferroelectric solid solutions. The PT phase has the highest T_C (763 K). Increasing the BT content of the samples reduces their T_C to 393 K. The addition of BZ to the samples causes not only a decrease in T_C but also a rather sharp broadening and a decrease in the height of the peak in $\varepsilon(T)$ near T_C (ε_m), producing features characteristic

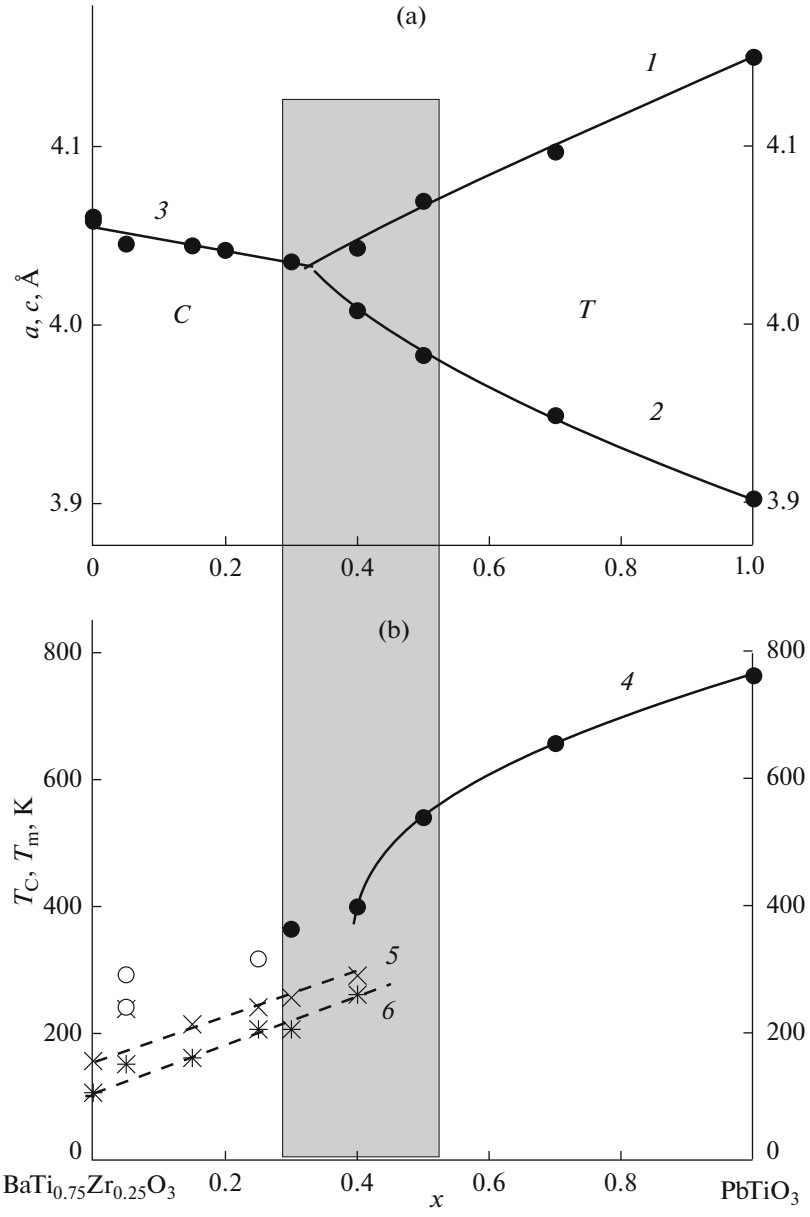

Fig. 4. Composition dependences of (a) the tetragonal (T) and cubic (C) unit-cell parameters [(*1*) a_T, (*2*) c_T, and (*3*) a_C], (b) (*4*) the Curie temperature T_C, and (*5*, *6*) the temperatures of the relaxation peaks, T_m, in the $\varepsilon(T)$ curves obtained at frequencies of 25 Hz and 1 MHz, respectively, for the $(1-x)BaTi_{0.75}Zr_{0.25}O_3 \cdot xPbTiO_3$ solid solutions with the perovskite structure. The shaded area corresponds to the coexistence of different solid solutions.

of ferroelectric relaxors and then of dielectric relaxors of the dipole glass type (Fig. 9a). The $\varepsilon(T)$ curves of the $(1-x)BZ \cdot xPT$ and $(1-x)BT_{0.5}Z_{0.5} \cdot xPT$ samples with $x < \approx 0.5$ and $x < \approx 0.4$ have a negligible ferroelectric peak (Figs. 6, 7, 9a).

The three peaks or breaks observed in the $\varepsilon(T)$ and $\tan\delta(T)$ curves of the samples close in composition to BT are obviously due to the phase transitions between the cubic (C) and tetragonal (T) phases at T_C, between the tetragonal and orthorhombic (O) phases at T_{TO}, and between the orthorhombic and rhombohedral (R) phases at T_{OR}, which are known to occur at $T_C = 393$ K, $T_{TO} = 278$ K, and $T_{OR} = 183$ K in BT [1, 3]. The addition of PT and BZ to BT lowers T_{TO} and T_{OR}, without significantly reducing the height of the peaks in $\varepsilon(T)$ or $\tan\delta(T)$ in the region of these phase transitions (Figs. 5, 8). At $y = 0.05$ and $x > 0.20$, these phase transitions do not show up in the $\varepsilon(T)$ or $\tan\delta(T)$ curve in the temperature range studied. The most likely reason for the sharp disappearance of these phase transitions

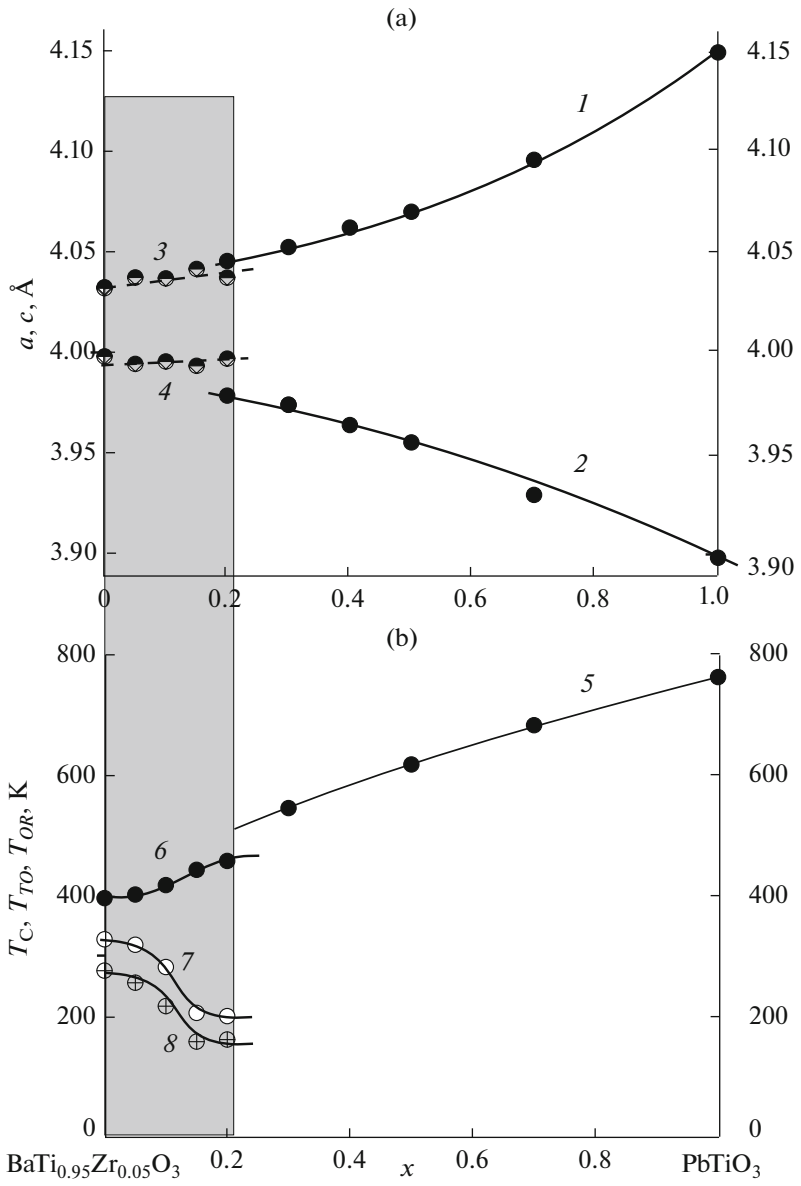

Fig. 5. Composition dependences of (a) the tetragonal (T) or pseudotetragonal cell parameters [(*1*, *3*) a_T, (*2*, *4*) c_T], (b) (*5*, *6*) the Curie temperature T_C, and (*7*, *8*) the phase transition temperatures T_{TO} and T_{OR}, respectively, for the $(1-x)BaTi_{0.95}Zr_{0.05}O_3 \cdot xPbTiO_3$ solid solutions with the perovskite structure. The shaded area corresponds to the coexistence of different solid solutions.

is that the composition of the samples falls in another phase field (Figs. 1, 5). Note that the O–R phase transition of the Zr-containing samples has signs of relaxor behavior: with increasing frequency, the position of the peak in $\tan\delta(T)$ markedly shifts to higher temperatures (Figs. 10e, 10f).

The two peaks with frequency-independent positions in the $\varepsilon(T)$ curves of the samples in which different solid solutions coexist and which undergo neither T–O nor O–R phase transition are most likely due to ferroelectric phase transitions.

The peaks in the $\varepsilon(T)$ and $\tan\delta(T)$ curves of the cubic solid solutions are located below room temperature. Increasing the BZ concentration in these samples increases the features characteristic of the behavior first of ferroelectric relaxors and then of dielectric relaxors of the dipole glass type: marked broadening of the peaks in the $\varepsilon(T)$ curves at T_m, the development of a pronounced frequency dispersion in ε and $\tan\delta$ for $T < T_m$, and the shift of the position of T_m to higher temperatures with increasing frequency (Figs. 9, 10).

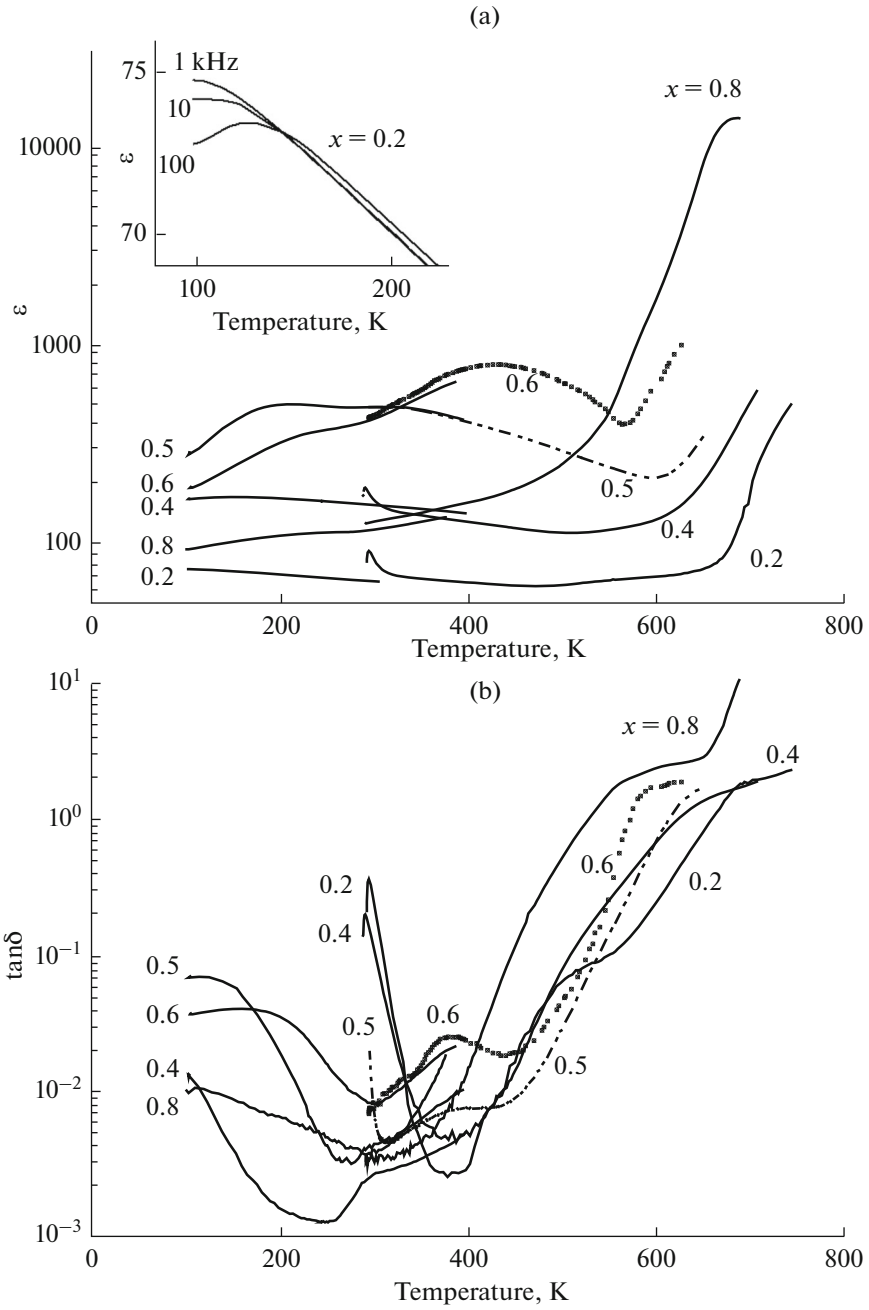

Fig. 6. Temperature dependences (a) $\varepsilon(T)$ and (b) $\tan\delta(T)$ measured at a frequency of 1 kHz for the $(1 - x)BaZrO_3 \cdot xPbTiO_3$ ceramic samples. Inset: $\varepsilon(T)$ data for the $x = 0.2$ sample at frequencies of 1, 10, and 100 kHz.

An interesting feature of the dielectric properties of the single-phase samples with $y \approx 0.2$–0.5 and $x \approx 0.05$–0.6 is that, unlike ordinary ferroelectric relaxors, they exhibit relaxor behavior not above [17] but below T_C (Figs. 9e, 9f, 10a–10d); that is, the first to form in them is an ordered ferroelectric state; as the temperature is lowered, they revert back to a disordered, relaxor state. Such behavior is characteristic of so-called reentrant relaxors [7]. It is due to competing interactions which tend to produce a long-range ferroelectric order or disorder in the arrangement of polar $[TiO_6]$ and nonpolar $[ZrO_6]$ octahedral groups, as well as in correlated and uncorrelated cation displacements from symmetric sites in the crystal structure of BTZ–PT (which refers especially to Pb^{2+} cations with an unshared $6s^2$ electron pair) [7–10].

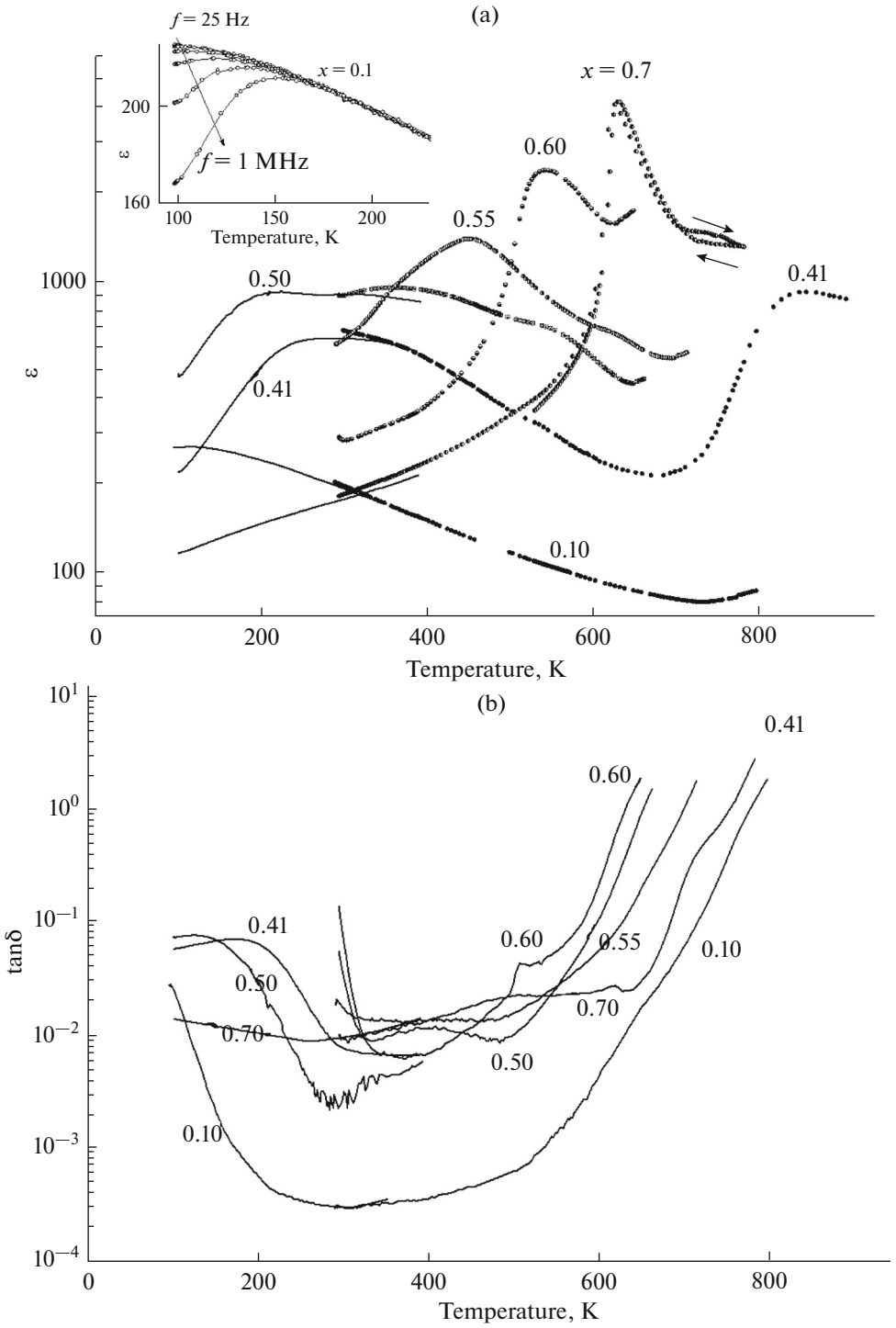

Fig. 7. Temperature dependences $\varepsilon(T)$ and $\tan\delta(T)$ measured at a frequency of 10 kHz for the $(1 - x)BaTi_{0.5}Zr_{0.5}O_3 \cdot xPbTiO_3$ ceramic samples. Inset: $\varepsilon(T)$ data for the $x = 0.1$ sample at frequencies from 25 Hz to 1 MHz.

CONCLUSIONS

Ceramic $(1 - x)Ba(Ti_{1-y}Zr_y)O_3 \cdot xPbTiO_3$ ($0 \le x, y \le 1$) samples have been prepared by solid-state reactions. According to X-ray diffraction data, the samples consist of perovskite solid solutions. The composition dependences of the unit-cell symmetry and parameters for the solid solutions have been used to map out the room-temperature phase diagram of the system in question. The results demonstrate that, in the composition regions adjacent to the BT–PT side and BZ cor-

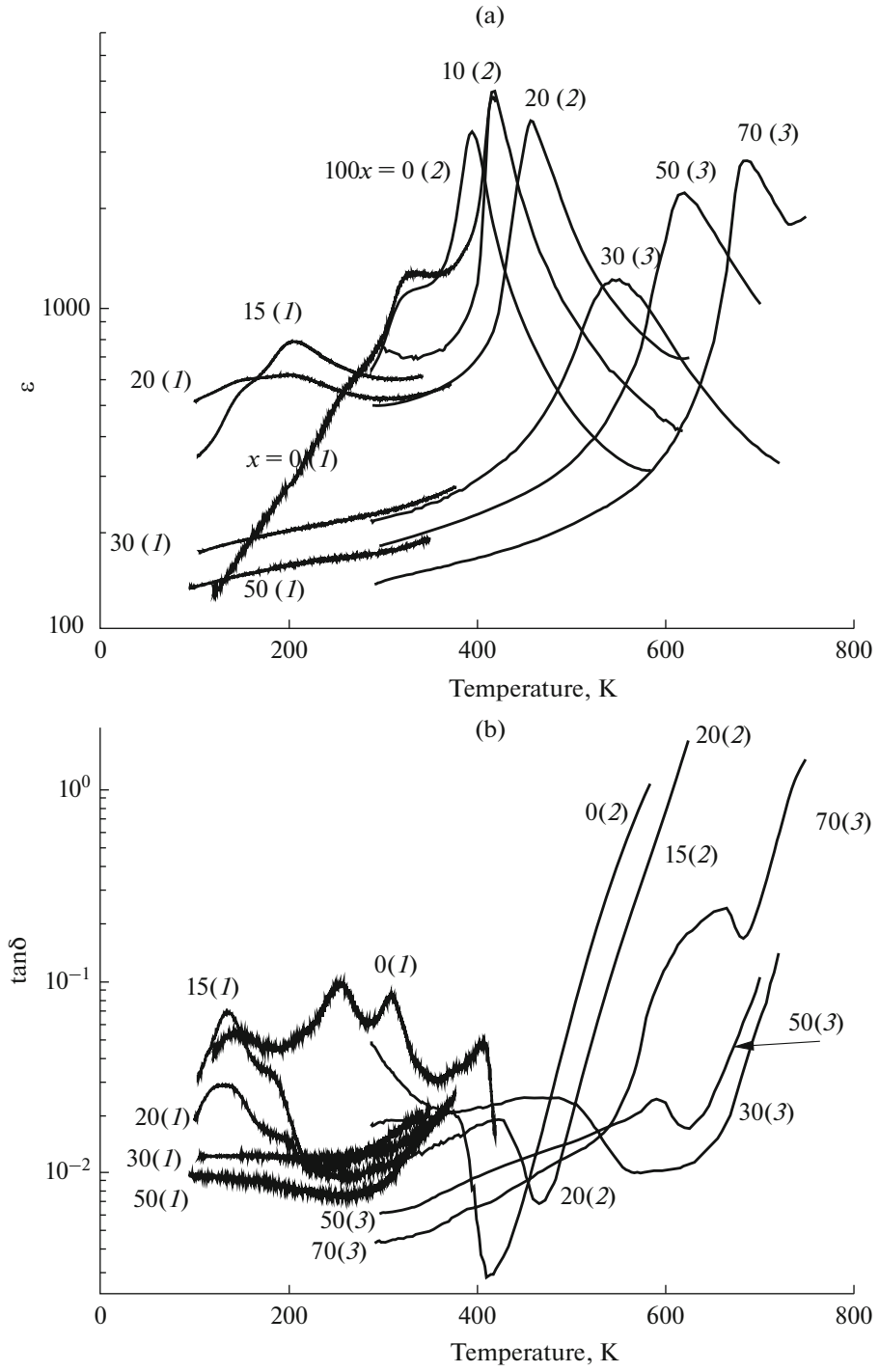

Fig. 8. Temperature dependences $\varepsilon(T)$ and $\tan\delta(T)$ measured at frequencies f = (*1*) 25 Hz, (*2*) 1 kHz, and (*3*) 1 MHz for the $(1-x)BaTi_{0.95}Zr_{0.05}O_3 \cdot xPbTiO_3$ ceramic samples. The numbers at the curves specify $100x$.

ner of the BT–BZ–PT composition triangle, the samples are single-phase and consist of tetragonal and cubic solid solutions, respectively. In the intermediate composition region, the samples consist of a mixture of different solid solutions with the perovskite structure.

The dielectric permittivity $\varepsilon(T,f)$ and dielectric loss tangent $\tan\delta(T,f)$ of the samples have been measured as functions of temperature and frequency in the temperature range 100–800 K and frequency range 25 to 10^6 Hz. The $\varepsilon(T)$ and $\tan\delta(T)$ curves have been found

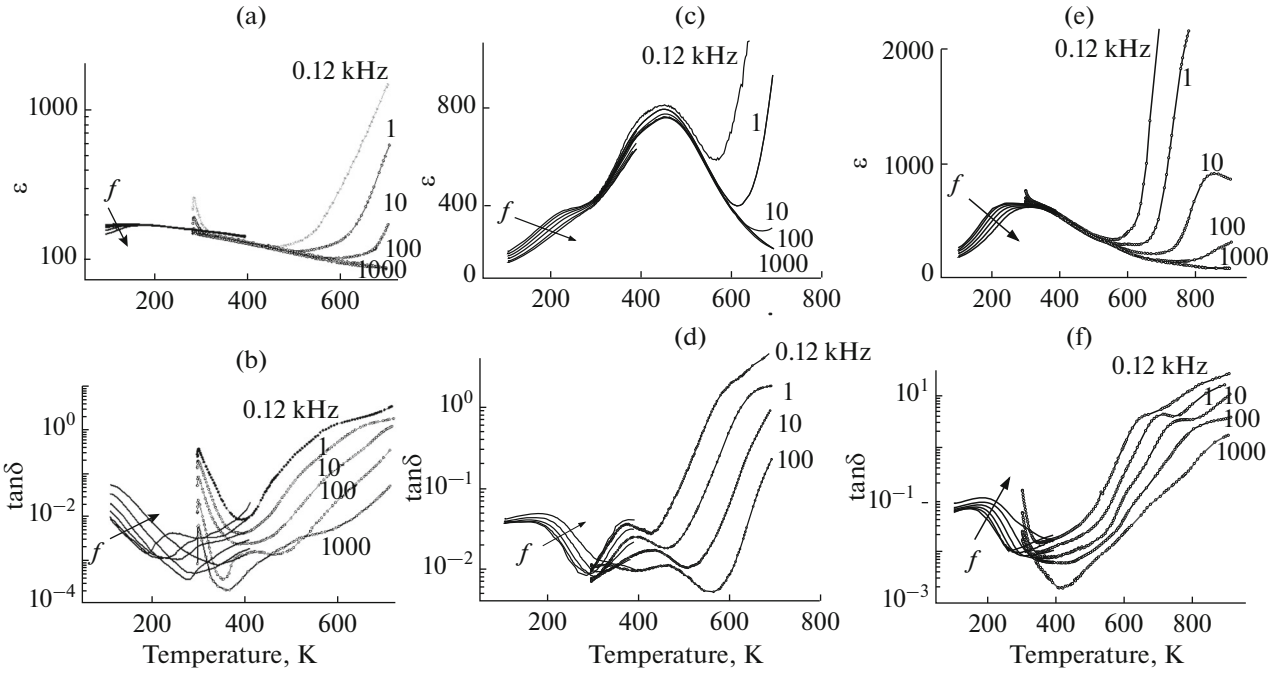

Fig. 9. Temperature dependences (a, c, e) $\varepsilon(T)$ and (b, d, f) $\tan\delta(T)$ measured at $f = 25$ to 10^6 Hz for the $(1-x)$BTZ · xPT samples: (a, b) $y = 1$, $x = 0.40$; (c, d) $y = 1$, $x = 0.60$; (e, f) $y = 0.50$, $x = 0.41$.

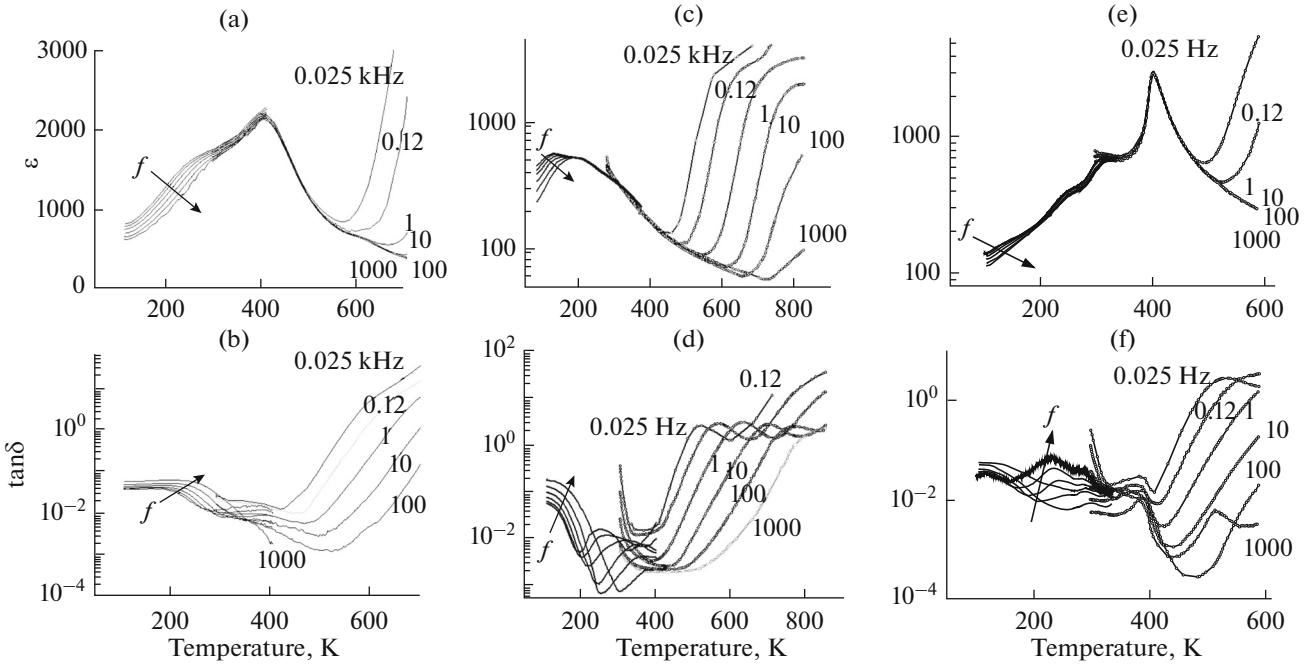

Fig. 10. Temperature dependences (a, c, e) $\varepsilon(T)$ and (b, d, f) $\tan\delta(T)$ measured at $f = 25$ to 10^6 Hz for the $(1-x)$BZT · xPT samples: (a, b) $y = 0.25$, $x = 0.40$; (c, d) $y = 0.30$, $x = 0.07$; (e, f) $y = 0.05$, $x = 0.05$.

to have one, two, or three prominent peaks reproducible in repeated measurements. The temperatures of the high-temperature peaks in ε, which are independent of the measuring field frequency, are the Curie points T_C of the ferroelectric solid solutions present in the samples. The highest T_C is offered by PT (763 K). The addition of BT to PT lowers T_C to 393 K, and the addition of BZ causes not only a decrease in T_C but

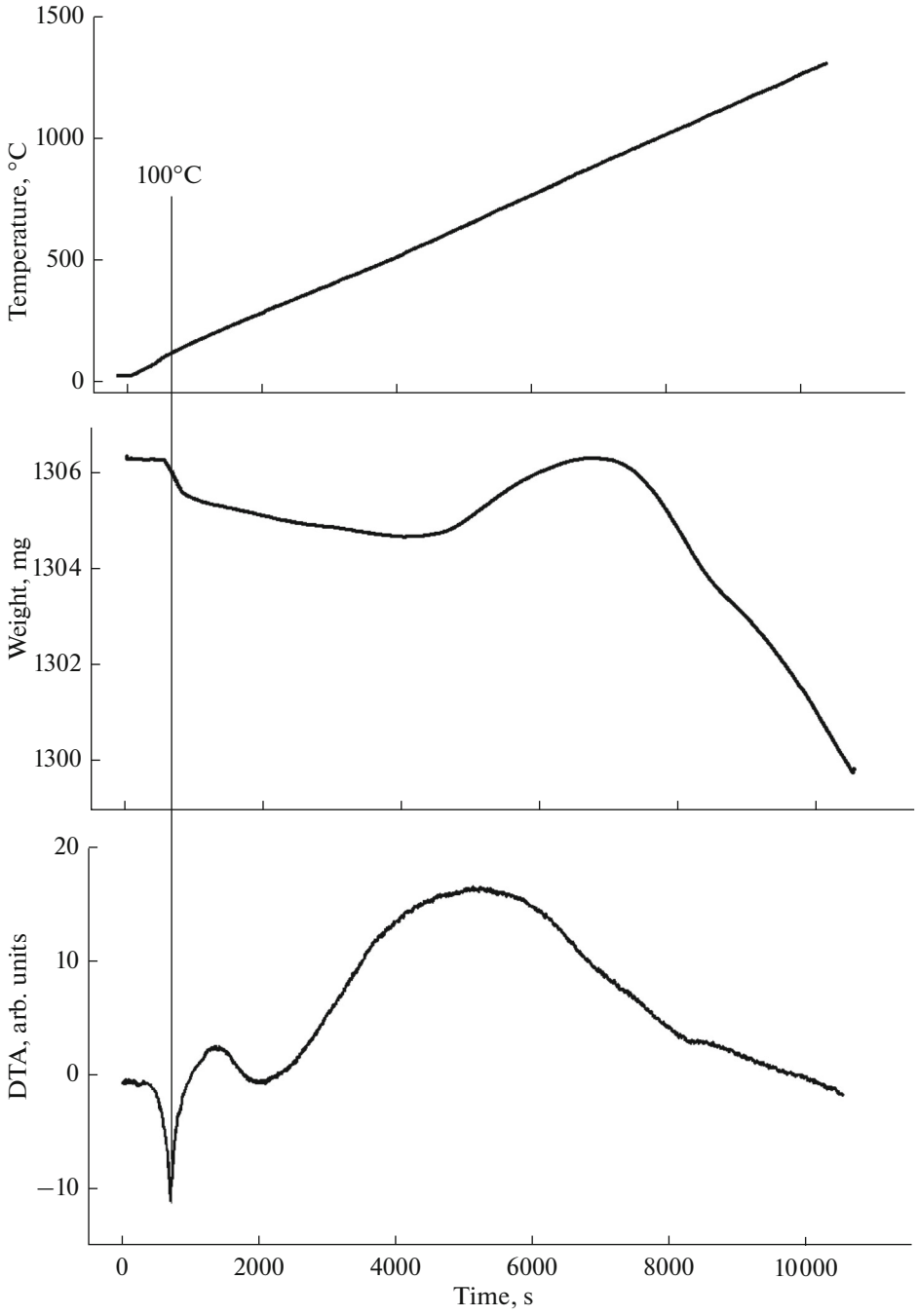

Fig. 11. Thermogravimetric analysis results for the $(1-x)Ba(Ti_{1-y}Zr_y)O_3 \cdot xPbTiO_3$ sample with $x = 0.41$ and $y = 0.50$.

also broadening and a decrease in the height of the peak in ε near T_C.

Substitutions of Pb for Ba and Zr for Ti in barium titanate reduce the temperatures T_{TO} and T_{OR} of the phase transitions between the tetragonal (*T*) and orthorhombic (*O*) phases and between the orthorhombic and rhombohedral (*R*) phases, without significantly reducing the height of the peaks in the ε(*T*) and $\tan\delta(T)$ curves near T_{TO} and T_{OR}. The reason for the sharp disappearance of these phase transitions with increasing PT content (at $y = 0.05$ and $x > 0.20$) is that the composition of the solid solutions falls in another phase field. The rise in T_C and the disappearance of the *T*–*O* and *O*–*R* phase transitions with increasing $PbTiO_3$ concentration in the samples improves the thermal stability of the room-temperature dielectric characteristics of the solid solutions.

The low-temperature peak at T_m in the ε of the samples that undergo no *T–O* or *O–R* phase transition has a relaxation nature. Its position shifts to higher temperatures with increasing frequency. Below T_m, there is a pronounced frequency dispersion in ε and tanδ. Increasing the BZ concentration in the samples causes first an increase in the relaxation peaks in ε and tanδ to a level characteristic of ferroelectric relaxors and then a decrease to a level typical of dielectric relaxors of the dipole glass type.

The $(1 - x)BT_{1-y}Z_y \cdot xPT$ samples with $y \approx 0.2$–0.5 and $x \approx 0.05$–0.6 exhibit behavior characteristic of so-called reentrant relaxors. Unlike ordinary ferroelectric relaxors, they exhibit relaxor behavior not above but below their ferroelectric Curie temperature.

ACKNOWLEDGMENTS

This work was supported by the Russian Federation Ministry of Education and Science (project no. 3.1099.2017/PCh) and the Russian Foundation for Basic Research (grant no. 15-02-04647a).

REFERENCES

1. Venevtsev, Yu.N., Politova, E.D., and Ivanov, S.A., *Segnetoelektriki i antisegnetoelektriki semeistva titanata bariya* (Ferro- and Antiferroelectrics of the Barium Titanate Family), Moscow: Khimiya, 1985.
2. Wu, T.B., Wu, C.M., and Chen, M.L., Highly insulative barium zirconate–titanate thin films prepared by rf magnetron sputtering for dynamic random access memory applications, *Appl. Phys. Lett.,* 1996, vol. 69, no. 18, pp. 2659–2661.
3. Rotenberg, B.A., *Keramicheskie kondensatornye dielektriki* (Ceramic Capacitor Dielectrics), St. Petersburg: Tipografiya OAO NII "Girikond", 2000.
4. Maiti, T., Guo, R., and Bhalla, A.S., Structure–property phase diagram of $BaZr_xTi_{1-x}O_3$ system, *J. Am. Ceram. Soc.,* 2008, vol. 91, no. 6, pp. 1769–1780.
5. Maiti, T., Guo, R., and Bhalla, A.S., Evaluation of experimental resume of $BaZr_xTi_{1-x}O_3$ with perspective to ferroelectric relaxor family: an overview, *Ferroelectrics,* 2011, vol. 425, no. 1, pp. 4–26.
6. Zhang, Q., Zhai, J., and Kong, L.B., Relaxor ferroelectric materials for microwave tunable applications, *J. Adv. Dielectr.,* 2012, vol. 2, no. 1, paper 1 230 002.
7. Shvartsman, V.V. and Lupescu, D.C., Lead-free relaxor ferroelectrics, *J. Am. Ceram. Soc.,* 2012, vol. 95, no. 1, pp. 1–26.
8. Nuzhnyy, D., Petzelt, J., Savinov, M., et al., Broadband dielectric response of $Ba(Zr,Ti)O_3$ ceramics: from incipient via relaxor and diffuse up to classical ferroelectric behavior, *Phys. Rev. B: Condens. Matter Mater. Phys.,* 2012, vol. 86, no. 1, pp 014 106.
9. Petzelt, J., Nuzhnyy, D., Savinov, M., Bovtun, V., Kempa, M., Ostapchuk, T., Hlinka, J., Canu, G., and Buscaglia, V., Broadband dielectric spectroscopy of $Ba(Zr,Ti)O_3$: dynamics of relaxors and diffuse ferroelectrics, *Ferroelectrics,* 2015, vol. 469, no. 1, pp. 14–25.
10. Petzelt, J., Nuzhnyy, D., Bovtun, V., Savinov, M., Kamba, S., and Hlinka, J., Lattice dynamics and dielectric spectroscopy of BZT and NBT lead-perovskite relaxors—comparison lead-based relaxors, *Phase Transitions,* 2015, vol. 88, no. 3, pp. 320–332.
11. Harris, N.H. and Tennery, V.J., Structural and dielectric investigation of the $PbTiO_3$–$BaZrO_3$ system, *J. Am. Ceram. Soc.,* 1967, vol. 50, no. 8, pp. 404–407.
12. Ikeda, T., Studies on (Ba–Pb)(Ti–Zr)O_3 system, *J. Phys. Soc. Jpn.,* 1959, vol. 14, no. 2, pp. 167–174.
13. Bush, A.A., Kamentsev, K.E., Stepanov, A.V., Karpunin, G.A., and Tatarintsev, K.B., Electrical properties of ceramic samples of $(1 - x)Ba(Ti_{1-y}Zr_y)O_3 \cdot xPbTiO_3$ solid solutions, *Inorg. Mater.,* 2017, vol. 53, no. 3, pp. 318–325.
14. Bera, J. and Rout, S.K., On the formation mechanism of $BaTiO_3$–$BaZrO_3$ solid solution through solid-oxide reaction, *Mater. Lett.,* 2005, vol. 59, no. 1, pp. 135–138.
15. *Powder Diffraction Files of the International Centre for Diffraction Data (ICDD),* 1999, file nos. 83-1880, 78-0299, and 06-0399.
16. Shannon, R.D., Revised effective ionic radii and systematic studies of interatomic distances in halides and chalcogenides, *Acta Crystallogr., Sect. A: Cryst. Phys., Diffr., Theor. Gen. Crystallogr.,* 1976, vol. 32, no. 5, pp. 751–767.
17. Bokov, A.A. and Ye, Z.-G., Recent progress in relaxor ferroelectrics with perovskite structure, *J. Mater. Sci.,* 2006, vol. 41, no. 1, pp. 31–52.

Translated by O. Tsarev